

1 **FUCCI tracking shows that Neurog3 levels vary with cell-cycle phase in endocrine-biased**
2 **pancreatic progenitors**

3 Matthew E. Bechard¹, Eric D. Bankaitis¹, Alessandro Ustione^{2,3}, David W. Piston^{2,3}, Mark A.
4 Magnuson^{1,2} and Christopher V.E. Wright^{1*}

5 ¹Vanderbilt University Program in Developmental Biology, Department of Cell and
6 Developmental Biology, Vanderbilt Center for Stem Cell Biology, Vanderbilt University School of
7 Medicine, Nashville, TN; ²Department of Molecular Physiology and Biophysics, Vanderbilt
8 University School of Medicine, Nashville, TN; ³Current address: Cell Biology and Physiology,
9 Washington University School of Medicine, St. Louis, MO

10 *Corresponding author. Email: chris.wright@vanderbilt.edu. Fax: +1 615 322 1917

11

12 **Abstract**

13 Neurog3^{HI} endocrine-committing cells are generated from a population of Sox9⁺ mitotic
14 progenitors with only a low level of *Neurog3* transcriptional activity (*Neurog3*^{TA,LO}). Low-level
15 Neurog3 protein, in *Neurog3*^{TA,LO} cells, is required to maintain their mitotic endocrine-lineage-
16 primed status. Herein, we describe a *Neurog3*-driven FUCCI cell-cycle reporter (*Neurog3*^{P2A,FUCCI})
17 derived from a *Neurog3* BAC transgenic reporter that functions as a loxed cassette acceptor
18 (LCA). In cycling Sox9⁺ *Neurog3*^{TA,LO} progenitors, the majority of cells in S-G₂-M phases have
19 undetectable levels of Neurog3 with increased expression of endocrine progenitor markers,
20 while those in G₁ have low Neurog3 levels with increased expression of endocrine
21 differentiation markers. These findings support a model in which variations in Neurog3 protein
22 levels are coordinated with cell-cycle phase progression in *Neurog3*^{TA,LO} progenitors with
23 entrance into G₁ triggering a concerted effort, beyond increasing Neurog3 levels, to maintain an
24 endocrine-lineage-primed state by initiating expression of the downstream endocrine
25 differentiation program prior to endocrine-commitment.

26

27 Introduction

28 *Neurogenin3* (*Neurog3*) encodes a bHLH transcription factor essential for endocrine-lineage
29 specification during mouse pancreas organogenesis (1). *Neurog3* is also critical to human
30 pancreatic endocrine-cell development, with null mutations causing neonatal diabetes, and
31 blocking β -cell differentiation from hESC (2). During mouse pancreatic development, high-level
32 *Neurog3* expression (*Neurog3^{HI}*) in Sox9⁺ pancreatic epithelial cells causes cell-cycle exit,
33 endocrine commitment and epithelial delamination (3–6). We recently demonstrated,
34 however, that low *Neurog3* levels are necessary for maintaining a population of Sox9⁺ *Neurog3*-
35 transcriptionally-active pancreatic epithelial cells in a mitotic endocrine-biased progenitor state
36 (defined as *Neurog3^{TA,LO}*), which pre-empts the transition to an endocrine-committed *Neurog3^{HI}*
37 state (6,7). Our findings presented a significant parallel to how a low level of *Neurog2* promotes
38 a neural-progenitor state while high levels cause neural differentiation and cell-cycle exit (8–
39 11). In those studies, higher Cdk activity in rapidly cycling progenitors, which have a relatively
40 short G₁, keeps *Neurog2* in a (hyper)-phosphorylated, unstable state that activates neural-
41 progenitor target genes (10,12). When the cell cycle of neural progenitors lengthens, however,
42 and G₁ lengthens, Cdk activity decreases, resulting in accumulation of a more stable (hypo)-
43 phosphorylated *Neurog2* that preferentially activates neural-differentiation targets (10,12).
44 Recently, we demonstrated that keeping *Neurog3* levels low leads to an increased mitotic index
45 of *Neurog3^{TA,LO}* progenitors and expands their numbers within the pancreatic epithelium (6).
46 Moreover, time-lapse observations show that the transition from the low level of *Neurog3*
47 observed in mitotic *Neurog3^{TA,LO}* progenitors to the high level necessary for endocrine-
48 commitment occurs ~3-6 hours after division of the parental *Neurog3^{TA,LO}* cell, during G₁ (6).

49 These findings led to our proposal that the level and stability of Neurog3 in mitotic Sox9⁺
50 *Neurog3*^{TA.LO} progenitors is regulated by the cell cycle and that G₁ extension promotes Neurog3
51 stabilization, accumulation, and endocrine commitment (**13**). Two recent reports support this
52 model, demonstrating that Neurog3 is targeted and destabilized by Cdks and that G₁
53 lengthening, by reducing Cdk activity, causes the accumulation of a more stable
54 un(der)phosphorylated form of Neurog3 (**14,15**).

55

56 We have been independently investigating if Neurog3 protein stability and progenitor
57 maintenance vs. endocrine differentiation decisions are connected to cell-cycle progression in
58 *Neurog3*^{TA.LO} progenitors. To do so, we used recombinase-mediated cassette exchange (RMCE)
59 to replace our previously described *Neurog3*^{RG} BAC transgenic reporter – which was designed as
60 a Loxed Cassette Acceptor (LCA) – with a *Neurog3*-driven single-transgene insert of the Fucci
61 (Fluorescence Ubiquitin Cell Cycle Indicator) reporter (*Neurog3*^{P2A.Fucci}). Our analysis of
62 *Neurog3*^{P2A.Fucci} reporter activity showed that in cycling Sox9⁺ *Neurog3*^{TA.LO} progenitors,
63 Neurog3 protein levels are highest during G₁ and lowest during S-G₂-M. Moreover, Sox9⁺
64 *Neurog3*^{TA.LO} progenitors in early G₁ show increased expression of downstream Neurog3 targets
65 usually associated with the forward passage into an endocrine commitment and progression
66 program. We propose that these findings support a model in which the endocrine-
67 differentiation program is already accessed, or preformed (albeit at a low or incomplete level),
68 in mitotic *Neurog3*^{TA.LO} progenitors prior to moving into endocrine-commitment. This work
69 provides a new tool for investigating, under *in vivo* conditions, Neurog3 and cell-cycle

70 connections in lineage-primed progenitors, and new insight on the role of Neurog3 in regulating
71 progenitor maintenance vs endocrine-commitment decisions.

72

73 **Results and Discussion**

74

75 ***Generating a Neurog3-driven P2A-fused single transgene FUCCI reporter.*** The FUCCI reporter
76 relies on cell-cycle-phase-dependent destruction of fluorescent proteins fused to “degradation
77 boxes” from hGeminin and hCdt, specifically the regions hGem^(1/110) and hCdt1^(30/120) (**16**),
78 allowing cell-cycle phase determination (Figure 1A). To investigate connections between
79 Neurog3 protein levels and cell-cycle progression in *Neurog3*^{TA.LO} progenitors we generated a
80 single mKO2-hCdt1^(30/120)-P2A-mVenus-hGem^(1/110) FUCCI (P2A.FUCCI) cassette, enabling both
81 FUCCI components to be expressed under the control of *Neurog3* (Figure 1B). We selected the
82 pairing of mKO2/mVenus because their fluorophores are spectrally separable from GFP and
83 mCherry, allowing P2A.FUCCI visualization in cells carrying our previously described *Neurog3*-
84 driven H2B^{mCherry}-P2A-GFP^{GPI} (*Neurog3*^{RG1} reporter) (**6**). As seen with the original FUCCI reporter
85 (**16**), *CMV*-driven expression of P2A.FUCCI in HeLa cells resulted in mKO2-hCdt1^(30/120) positivity
86 during G₁ and mVenus-hGem^(1/110) positivity during S-G₂-M, with a brief overlap of the two
87 fusion proteins during the G₁/S phase transition (Figure 1B).

88

89 To facilitate generating additional *Neurog3* BAC transgenic reporters from the *Neurog3*^{RG}
90 reporter, we had flanked the *Neurog3*^{RG} cassette with tandem *lox71* and *lox2272* sites, making
91 a Loxed Cassette Acceptor (LCA) allele (see ref. **6**; Figure 2A). This design was to allow
92 *Neurog3*^{RG} to be replaced with any *lox66/lox2272*-flanked cassette via RMCE in mESCs. To avoid

93 potential issues with performing RMCE in cells carrying multiple LCA alleles, mESCs identified as
94 having stably integrated the *Neurog3*^{RG} BAC LCA transgene were screened for single-copy
95 insertion by a qPCR-based assay (see methods and materials; Figure 2B and C) that accurately
96 estimates transgene copy number (17). Using this assay, two mESC transgenic clones, referred
97 to as *Neurog3*^{RG1} and *Neurog3*^{RG2}, were identified as having copy numbers of 1.25 ± 0.16 and
98 1.46 ± 0.26 (Figure 2C). Derivation of *Neurog3*^{RG} mESC lines and the subsequent *Neurog3*^{RG1}
99 mouse line are described in (6). As with the *Neurog3*^{RG1} mouse (6), examination, in *Neurog3*^{RG2}
100 mice, of gross tissue and islet architecture, ad libitum fed glucose levels, and proportions of
101 Sox9⁺ *Neurog3* protein-low (*Neurog3*^{PL0}) versus Sox9⁻ *Neurog3* protein-high (*Neurog3*^{PHI}) cells
102 during pancreas development, revealed no abnormal phenotype (Figure 2-figure supplement
103 1A-D; data not shown). We next validated the LCA function of the *Neurog3*^{RG} BAC transgene by
104 using the *Neurog3*^{RG2} mESC line to derive a *Neurog3*^{P2A.FUCCI} mESC line. A lox66/lox2272-flanked
105 *Neurog3*^{P2A.FUCCI}-PGK-hygro^R cassette was generated with cassette placement mimicking that of
106 *Neurog3*^{RG} (Figure 2-figure supplement 2A). Following RMCE in *Neurog3*^{RG2} mESCs, PCR was
107 performed to verify replacement of the lox71/lox2272-flanked *Neurog3*^{RG}-PGK-Puro^{ATK} cassette
108 with the lox66/lox2272 *Neurog3*^{P2A.FUCCI}-PGK-hygro^R cassette (Figure 2-figure supplement 2B).
109 This derivative *Neurog3*^{P2A.FUCCI} mESC line was then used to generate *Neurog3*^{P2A.FUCCI} transgenic
110 mice. Given that the genomic integration site is likely different in *Neurog3*^{RG2} vs. *Neurog3*^{RG1}
111 mESC lines, we used *Neurog3*^{RG2} mESCs to derive *Neurog3*^{P2A.FUCCI} mice to allow future breeding
112 of *Neurog3*^{P2A.FUCCI} to *Neurog3*^{RG1} mice to enable four-color reporting of cell-cycle phase and
113 *Neurog3* expression. Our proposal is that such visualization could facilitate experiments aimed
114 at understanding if, like other progenitor populations, G₁ length or overall cell-cycle length in

115 mitotic *Neurog3*^{TA.LO} progenitors plays a role in regulating progenitor maintenance vs.
116 endocrine-commitment decisions, or even in determining whether one endocrine cell-type is
117 produced over another at specific stages or locations within the developing pancreas.

118

119 ***Neurog3 levels and progenitor maintenance vs. endocrine-commitment decisions are coupled***

120 ***to the cell cycle.*** Recent studies showed that during S-G₂-M, Neurog3 is kept in a

121 hyperphosphorylated unstable state via Cdk phosphorylation, and that decreased Cdk activity

122 associated with entrance into G₁ result in stabilization and accumulation (14,15). These findings

123 support our model that, in actively cycling *Neurog3*^{TA.LO} progenitors, Neurog3 protein levels

124 vary according to the cell-cycle phase (13). To address this issue, we used *Neurog3*^{P2A.FUCCI}

125 reporter expression in *Neurog3*^{TA.LO} progenitors to track cell-cycle progression in relation to

126 Neurog3 protein levels. Previously, *Neurog3*^{TA.LO} progenitors were defined as a population of

127 Sox9⁺ *Neurog3*-transcriptionally active (low-level *Neurog3*^{RG1} reporter expression) progenitors

128 comprising cells with either low (*Neurog3*^{TA.pLO}) or immunologically undetectable Neurog3

129 (*Neurog3*^{TA.pUD}) (6). Consistent with this definition, *Neurog3*^{TA.LO} progenitors were herein

130 defined as Sox9-positive and positive for either component of the *Neurog3*^{P2A.FUCCI} reporter,

131 with low or undetectable Neurog3 protein, whereas endocrine-committed *Neurog3*^{TA.HI} cells

132 should be Sox9-negative, Neurog3^{pHI} and positive for mKO2-hCdt1^(30/120) (Figure 3A).

133 Unexpectedly, we detected significant residual cytoplasmic mVenus-hGem^(1/110) fluorescence in

134 post-mitotic, actively delaminating, endocrine-committed *Neurog3*^{TA.HI} cells that showed the

135 expected high mKO2-hCdt1^(30/120) signal (Figure 3A). This observation was different from

136 previous reports on the FUCCI reporter, where mVenus-hGem^(1/110) was mostly degraded after

137 M-phase, becoming absent by the time of mKO2-hCdt^(30/120) detection in early G₁ (**16,18**). This
138 cytoplasmic mVenus-hGem^(1/110) signal, however, was completely absent in islets (data not
139 shown), which could suggest that high *Neurog3*^{P2A.FUCCI} reporter expression in delaminating
140 *Neurog3*^{TA.HI} cells overwhelms the ubiquitin-mediated protein degradation pathway, extending
141 the time necessary to fully degrade mVenus-hGem^(1/110) after entering G₁. We were therefore
142 careful to score *Neurog3*^{P2A.FUCCI} cells as only in S-G₂-M if definitively nuclear mVenus signal was
143 observed, with no indication of mKO2 (Figure 3A). By these criteria, the majority of Sox9⁺
144 *Neurog3*^{TA.LO} cells were in S-G₂-M and thus mitotic, while nearly all *Neurog3*^{TA.HI} cells were in G₁
145 (Figure 3B). To determine if Neurog3 protein levels vary through the cell cycle, we examined
146 the cell-cycle status of Sox9-positive *Neurog3*^{TA.pLO} versus *Neurog3*^{TA.pUD} cells. Quantification
147 revealed that 78% (± 8.1%) of *Neurog3*^{TA.pUD} cells were in S-G₂-M and 22% (± 8.1%) in G₁ (Figure
148 3B). Although stabilization and accumulation of Neurog3 occurs during G₁, previous work
149 showed that Neurog3 protein is present during S phase, with rapid degradation occurring
150 during G₂-M (**14**). Corroborating that result, we show that while the majority (55% ± 3.6%) of
151 Sox9⁺ *Neurog3*^{TA.pLO} cells were in G₁, 45% (± 3.6%) were in S-G₂-M (Figure 3B). These findings
152 show that the Neurog3 protein level in cycling Sox9⁺ *Neurog3*^{TA.LO} progenitors is lowest during
153 S-G₂-M and highest during G₁.

154

155 Previous work shows that a low Neurog3 protein level maintains a mitotic, endocrine lineage-
156 primed progenitor state (**1,4–7**). Given the cell-cycle-dependent variation of Neurog3 protein
157 level, we hypothesized that the low-level accumulation of Neurog3 in *Neurog3*^{TA.LO} progenitors
158 in G₁ could trigger gene expression changes that were consistent with endocrine lineage-

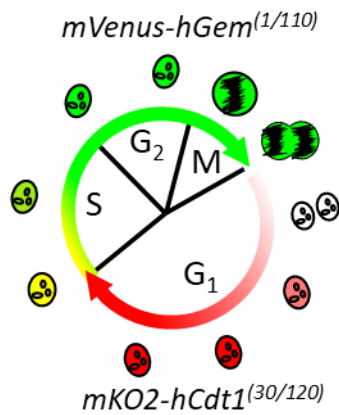
159 priming, and involving genes other than solely *Neurog3*. Therefore, intraepithelial
160 *Neurog3*^{P2A.FUCCI+} cells (*Neurog3*^{TA.LO} progenitors) were isolated from E14.5 *Neurog3*^{P2A.FUCCI}
161 pancreatic explants by flow sorting of lumen-contacting (Muc1⁺) cells, then sorting cells in S-G₂-
162 M (mKO2⁻ mVenus⁺) or G₁ (mKO2⁺ mVenus⁻) (Figure 4A). As described above, actively
163 delaminating *Neurog3*^{TA.HI} cells display relatively bright, yet to be degraded, cytoplasmic
164 mVenus and high nuclear mKO2 (Figure 3A). To exclude this population, the flow-cytometry
165 gating was set so that mVenus/mKO2 co-positive cells were not collected (Figure 4A). Analysis
166 via qRT-PCR showed that while in S-G₂-M, *Neurog3*^{TA.LO} progenitors are enriched for *Sox9* and
167 *Hes1* (mitotic endocrine-progenitor markers) with low expression of *Neurog3* and several
168 markers indicating forward progression towards endocrine commitment and further
169 differentiation (*NeuroD1*, *Insm1*, *Glucagon*, *Insulin*) (Figure 4B). *Neurog3*^{TA.LO} progenitors in G₁,
170 however, showed significantly decreased *Hes1* and increased *Neurog3*, *NeuroD1*, *Insm1*,
171 *Glucagon* and *Insulin* (Figure 4B). Despite the increases in endocrine-commitment markers,
172 entrance into G₁ did not significantly alter *Sox9* expression (Figure 4B), demonstrating that
173 these cells are intraepithelial *Neurog3*^{TA.LO} progenitors. The data are also consistent with the
174 idea that cells in this mitotic progenitor state, when in G₁, initiate expression of several genes
175 representing the downstream endocrine differentiation program, at a stage prior to
176 commitment. Given the role of *Neurog3* in trans-activating *NeuroD1* and *Insm1* (19–21), we
177 speculate that the low-level accumulation of *Neurog3* specifically in G₁ could be sufficient to
178 induce low-level *NeuroD1/Insm1* expression in lineage-primed progenitors. It is also possible
179 that signals initiating the lineage-primed state activate low-level expression of other
180 transcription-factor genes in a *Neurog3*-independent manner. It is plausible that the concerted

181 expression of several trans-acting factors establishes a relatively weak or incomplete form of
182 the GRN that is normally considered to work only in post-mitotic committed cells. It would be
183 important to discover if entrance into G₁ were also linked to alterations in chromatin
184 architecture and DNA accessibility that allow low-level expression of GRN member genes
185 contributing to lineage priming in *Neurog3*^{TA.LO} progenitors. Understanding how cell-cycle
186 progression regulates such gene expression programs could lead to understanding if the final
187 hormone-secreting cell fate might become preconditioned in the mitotic lineage-biased stage,
188 and possibly how to manipulate cells at this early phase of their lifespan to improve the
189 generation of functional endocrine cells.

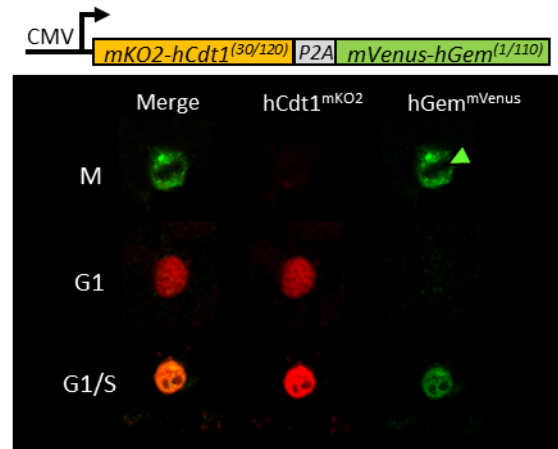
190

191

A



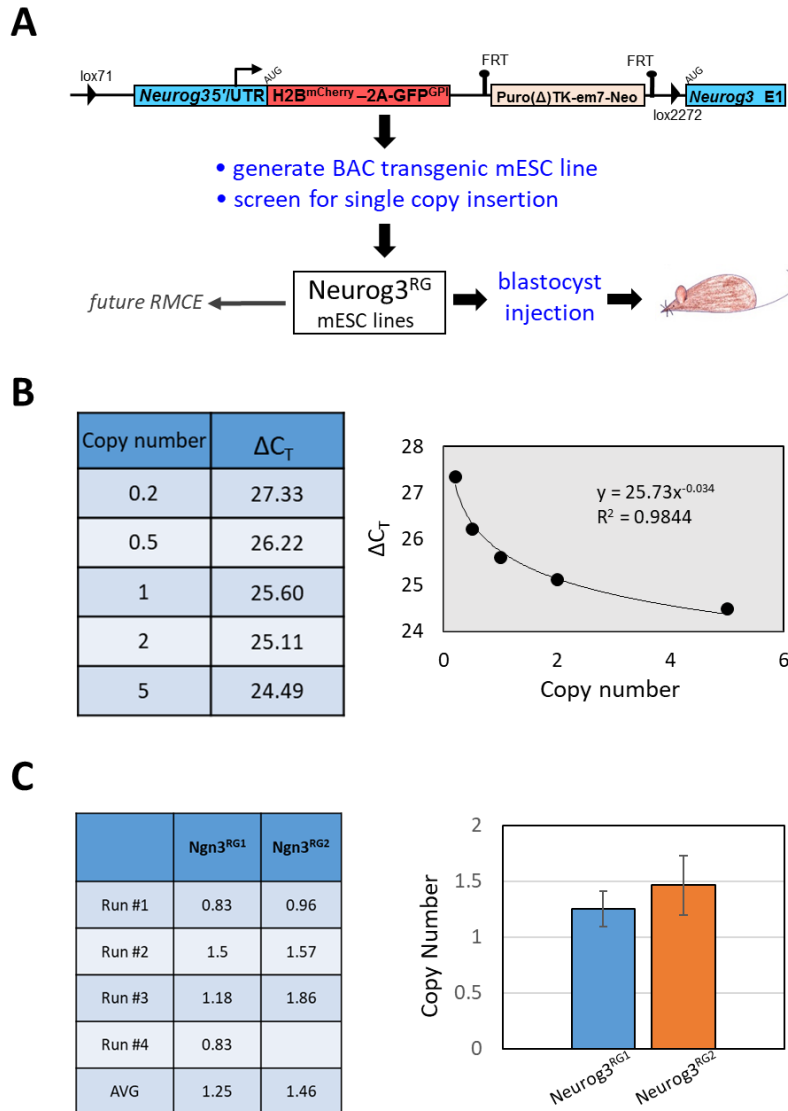
B



192

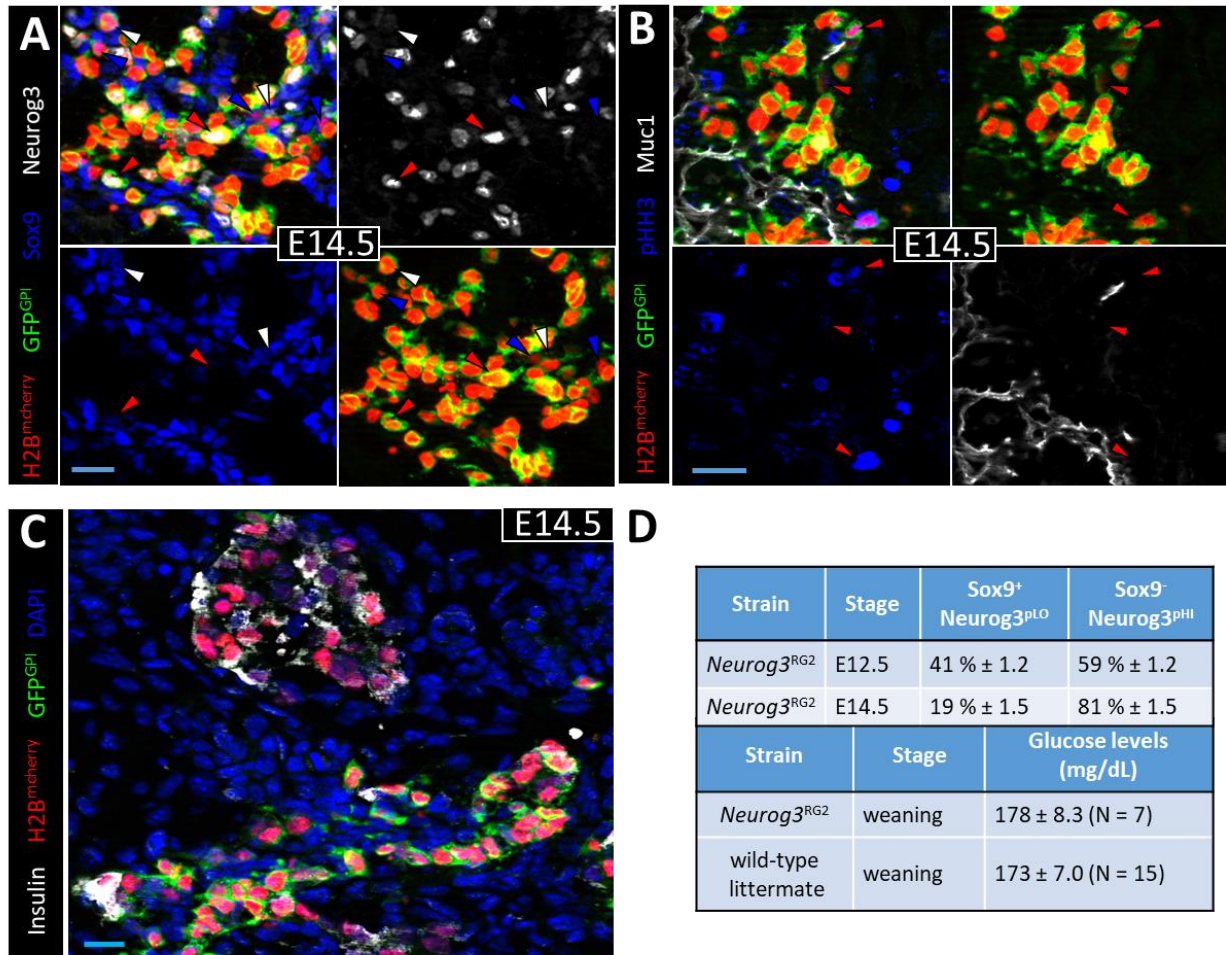
193 **Figure 1:** Peptide-2A single-transgene FUCCI transgene. (A) Diagram (adapted from Sakaue-Sawano et
194 al., 2008) indicating phases of the cell cycle marked by the components of the FUCCI reporter: mVenus-
195 hGem^(1/110) (S-G₂-M) and mKO2-hCdt1^(30/120) (G₁). (B) *Top*, Diagram of CMV^{P2A.FUCCI} expression plasmid.
196 *Bottom*, Immunofluorescence images showing CMV^{P2A.FUCCI} reporter expression in HeLa cells at
197 appropriate stages of the cell cycle. Green arrowhead indicates mitotic chromosomes.

198



199

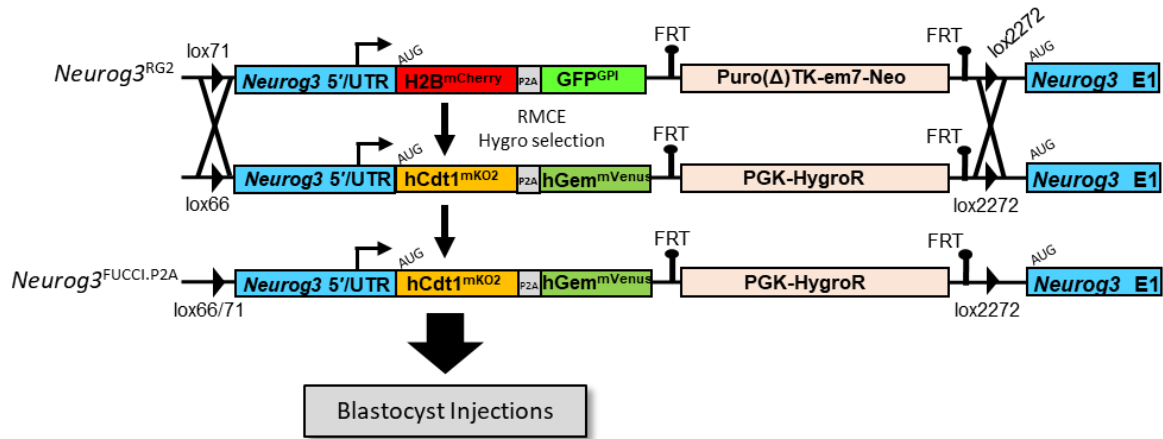
200 **Figure 2:** Generation of an LCA-capable BAC transgenic *Neurog3*^{RG} mESC line. (A) Schematic detailing the
 201 generation of transgenic mES cell lines carrying a single copy of a *Neurog3*^{RG} BAC transgene designed to
 202 serve as an LCA in future RMCE reactions. The *Neurog3*^{RG} BAC transgenic mESCs were previously used to
 203 generate *Neurog3*^{RG} reporter mice (6). *Neurog3* 5'/UTR represents the region 5' of the start codon
 204 containing cis regulatory elements and the *Neurog3* 5' untranslated region (UTR). (B) Table and graph of
 205 a standard curve, generated via a qPCR-based assay (see methods and materials), that relates transgene
 206 copy number to a specific ΔC_T value. (C) Table and graph depicting the estimated *Neurog3*^{RG} BAC
 207 transgene copy number present in *Neurog3*^{RG1} and *Neurog3*^{RG2} mESC lines.



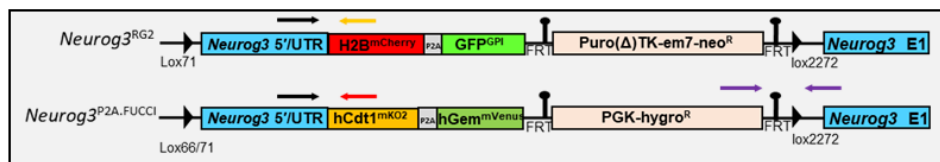
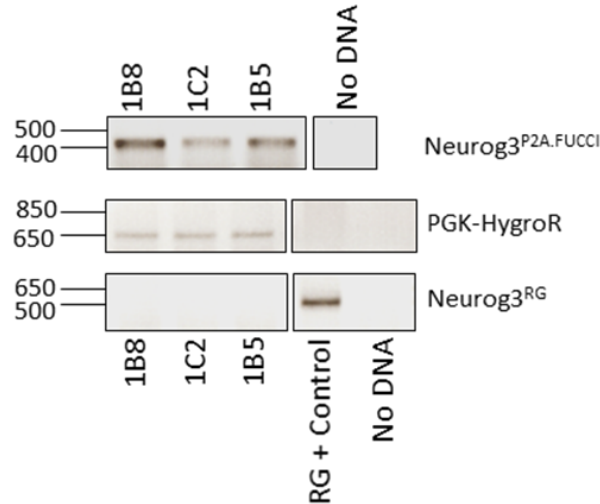
208

209 **Figure Supplement 1: *Neurog3*^{RG2} BAC transgenic reporter is a passive reporter.** (A) E14.5 pancreatic
 210 epithelium showing H2B^{mCherry}, GFP^{GPI}, Sox9 and Neurog3. Blue, white and red arrowheads indicate Sox9⁺
 211 *Neurog3*^{TA.pUD} cells, Sox9⁺ *Neurog3*^{TA.pLO} cells and Sox9⁻ *Neurog3*^{TA.HI} cells, respectively. (B) E14.5
 212 pancreatic epithelium showing H2B^{mCherry}, GFP^{GPI}, Muc1, and phospho-Histone H3 (pHH3). Red
 213 arrowheads indicate pHH3⁺ Muc1⁺ *Neurog3*^{TA.LO} cells. (C) Image of Islets of Langerhans and the
 214 pancreatic epithelium at E14.5 showing H2B^{mCherry}, GFP^{GPI}, Insulin and DAPI. (D) Top table details
 215 percentage of Sox9⁺ Neurog3^{pLO} vs. Sox9⁻ Neurog3^{pHI} cells in *Neurog3*^{RG2+} pancreatic epithelium at e12.5
 216 and e14.5, which are unchanged relative to typical analyses of pancreata from wild-type mice (5).
 217 Bottom table details blood glucose levels, measured in whole blood using a Nova Max Plus glucose
 218 meter and test strips, of ad libitum fed wild-type and *Neurog3*^{RG2+} mice at weaning (~P21). Bars, 20 μm.

A

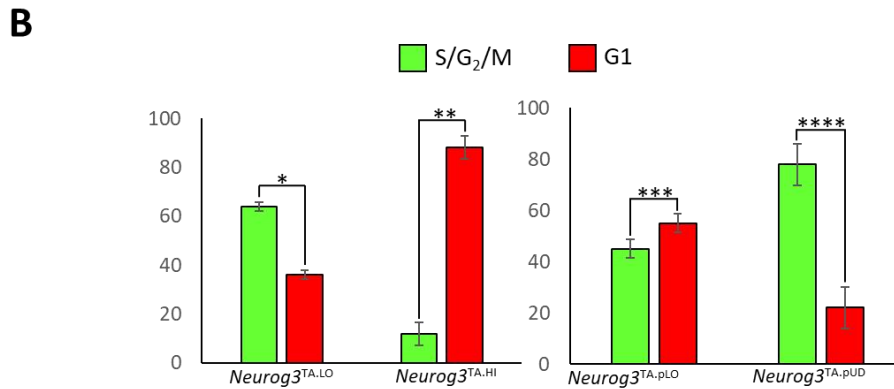
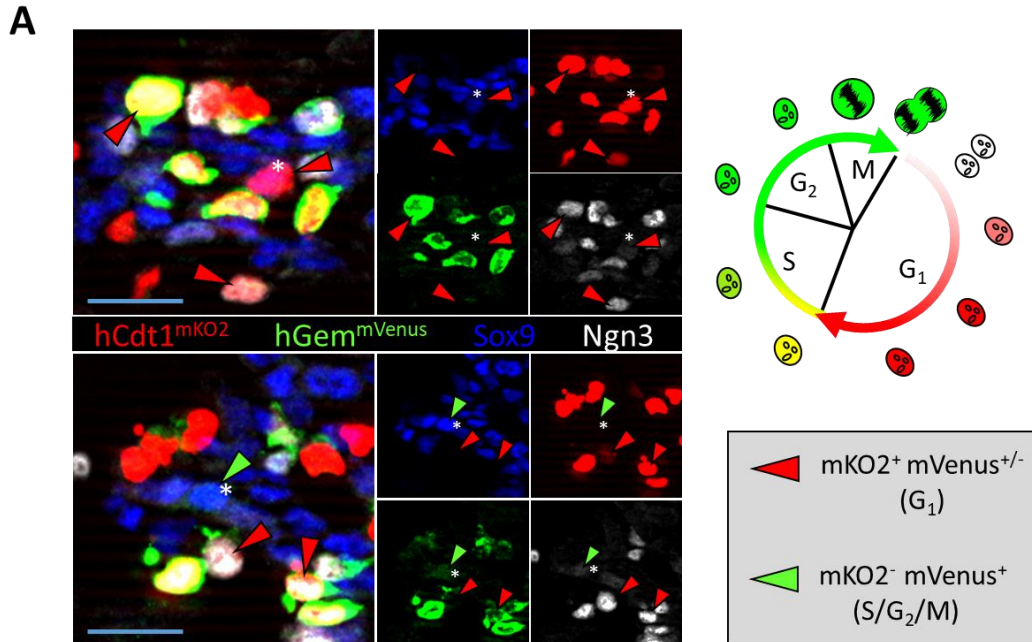


B



219

220 **Figure Supplement 2: RMCE-mediated derivation of *Neurog3*^{P2A.FUCCI} mESC line.** (A) Scheme for using
 221 RMCE to replace the LCA-capable *Neurog3*^{RG} BAC transgenic reporter with the Lox66/lox2272-flanked
 222 *Neurog3*^{P2A.FUCCI} transgenic reporter. (B) Top, PCR of genomic DNA from three mES cell lines (1B8, 1C2,
 223 1B5) to check for successful RMCE of the lox71/lox2272-flanked *Neurog3*^{RG} cassette in *Neurog3*^{RG2}
 224 mESCs for the lox66/lox2272-flanked *Neurog3*^{P2A.FUCCI} cassette. Bottom, schematic showing the
 225 approximate binding sites for the *Neurog3*^{RG}, *Neurog3*^{P2A.FUCCI} and PGK-hygro^R primer pairs.



226

227 **Figure 3:** Neurog3 protein levels vary according to cell-cycle phase. (A) E14.5 pancreatic epithelium

228 showing Sox9, Neurog3, hCdt1^{mKO2} and hGem^{mVenus}. Red arrowheads indicate Neurog3^{P2A.FUCCI+} cells that

229 are mKO2⁺ and thus in G₁, green arrowheads indicate Neurog3^{P2A.FUCCI+} cells that are mVenus⁺ and thus in

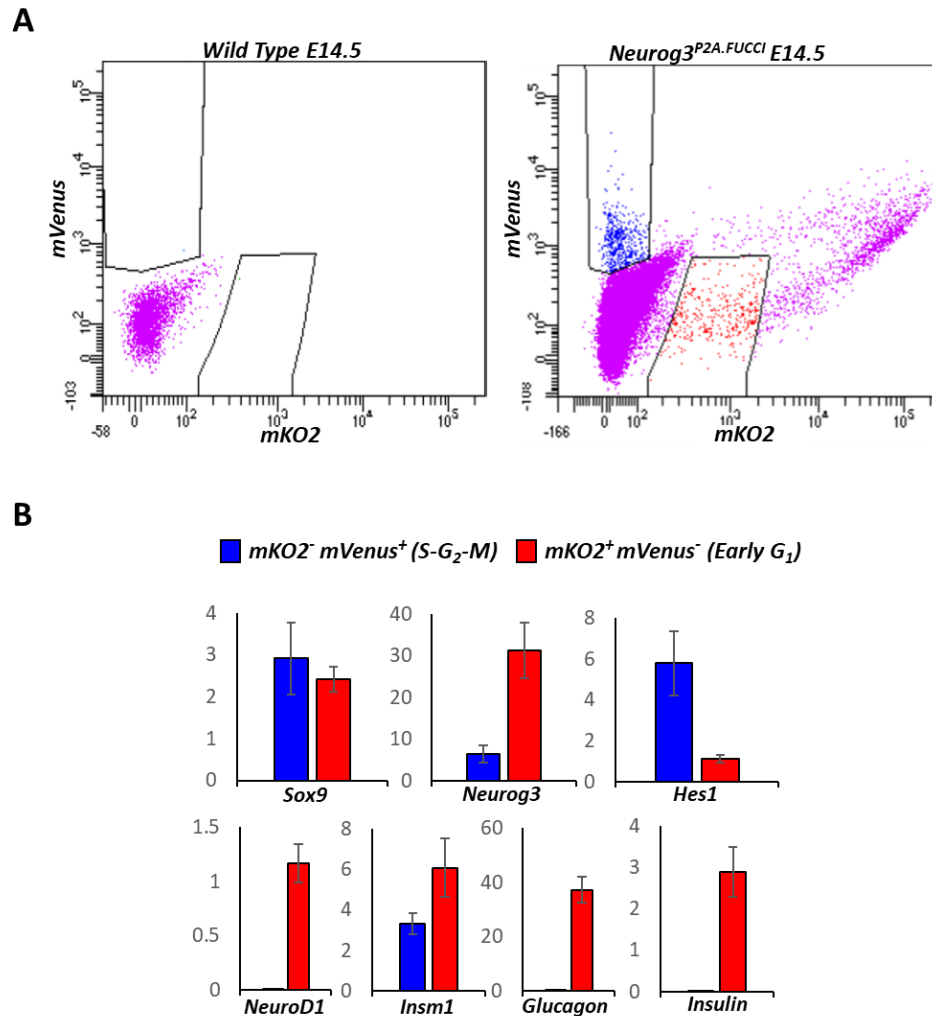
230 S-G₂-M phase. Asterisk indicates Sox9⁺ Neurog3^{TA,LO} cells, arrows with no asterisk indicate Sox9⁻

231 Neurog3^{TA,HI} cells. (B) Left, percentage of Sox9⁺ Neurog3^{TA,LO} and Sox9⁻ Neurog3^{TA,HI} cells in S-G₂-M versus

232 G₁ phase. Right, percentage of Sox9⁺ Neurog3^{TA,pLO} and Sox9⁺ Neurog3^{TA,pUD} in S-G₂-M versus G₁ phase. (*n*

233 = 1600, *N* = 3). (*) *P* = 0.0072; (**) *P* = 4 × 10⁻⁶; (***) *P* = 0.0607; (****) *P* = 0.0039. Data are mean ± SEM.

234 Bars, 20 μm.



235

236 **Figure 4:** Neurog3 promotes low-level activation of downstream targets during G₁ in the mitotic

237 *Neurog3*^{TA,LO} progenitor state. (A) flow cytometry plot detailing capture of lumen-apposed (Muc1⁺)

238 *Neurog3*^{P2A.FUCCI+} cells in S-G₂-M (mKO2⁻ mVenus⁺) (Blue population) or G₁ (mKO2⁺ mVenus⁻) (red

239 population) from E14.5 *Neurog3*^{P2A.FUCCI} pancreata. Flow-sorted cells were collected into TRIzol for RNA

240 isolation and cDNA synthesis. (B) Relative expression level (y-axis), normalized to *Gapdh*, of *Sox9*,

241 *Neurog3*, *Hes1*, *NeuroD1*, *Insm1*, *glucagon*, and *Insulin* for E14.5 flow captured Muc1⁺ *Neurog3*^{P2A.FUCCI+}

242 mKO2⁻ mVenus⁺ (blue bars) and Muc1⁺ *Neurog3*^{P2A.FUCCI} mKO2⁺ mVenus⁻ (red bars) cells. Each data point

243 represents an average of at least three technical replicates. Error bars are SEM. See supplemental

244 table 1 for a list of primers used.

245 **Supplemental Table 1.** Primers used for genotyping and qRT-PCR analyses.

Genotyping Primers			
Target	Primer name	Sequence	
Ngn3^{RG2}	H2BFv3	5'-GAGGCTCAGCTATCCACTGC-3'	
	H2BRv3	5'-GAATTCATGATGCCCATGGC-3'	
Ngn3^{P2A.FUCCI}	H2BFv3	5'-GAGGCTCAGCTATCCACTGC-3'	
	FUCCI-R3	5'-GGCTTATATGCGCACTGAC-3'	
HygroR	pHyS6	5'-CCGATGGCTGTGTAGAAGTACTCG-3'	
	P1FNR	5'-GATGGTGAGCGCATCCAAG-3'	
qRT-PCR Primers			
<i>GAPDH</i>	5'-ACTTTGGCATTGTGGAAGG-3'	<i>Glucagon</i>	5'-ACATCTCGTGCCAGTCACTT-3'
	5'-GGATGCAGGGATGATGTTCT-3'		5'-CGTTGGGTTACACAATGCT-3'
<i>Sox9</i>	5'-CTCCCCCTTTCTTTGTTGTTT-3'	<i>Hes1</i>	5'-TAGCCACCTCTCTTCTGAC-3'
	5'-TCTGAAACCTCTCATTTGTCCA-3'		5'-CAGTGCATGGTCAGTCACTTAAT-3'
<i>Ngn3</i>	5'-CAGGGTTTCTGAGCTTCTCC-3'	<i>Insulin</i>	5'-CAGCAAGCAGGTCATTGTTT-3'
	5'-GGGAAGGGTAACGACTTGAA-3'		5'-GGGACCACAAAGATGCTGTT-3'
		<i>NeuroD1</i>	5'-GAAGATTGATCCGTGGCTTT-3'
			5'-CAGCATCAATGGCAACTTCT-3'

246

247

248

249

250

251

252

253

254 **Supplemental Table 2.** Antibodies and detection methods.

Primary Antibodies				
Antigen	Species	Dilution	Label Method	Source
Muc1	Hamster	1:250	IF	NeoMarkers
Sox9	Rabbit	1:2500	IF	Millipore
Neurog3	Goat	1:40,000	IF	G. Gu (Vanderbilt)
pHH3	Rabbit	1:500	IF	Millipore
EGFP/Venus	Rabbit	1:500	IF	Clontech Aves
	Chicken	1:500	IF	
Insulin	Guinea Pig	1:500	IF	Dako
DAPI	----	----	Mount Media	Life Technologies
Secondary Antibodies				
Antigen	Conjugation	Dilution	Source	
Rabbit/Chicken	Cy2	1:250	Jackson ImmunoResearch	
Guinea pig/ Goat Hamster	Cy5	1:250	Jackson ImmunoResearch	
Rabbit	405	1:250		
Goat	Biotinylated	1:250	Vector Laboratories	

255

256

257

258

259 **Materials and Methods**

260

261 **Mice and transgene copy number analysis**

262 Animal protocols were approved by the Vanderbilt University Institutional Animal Care and Use
263 Committee. All animals were PCR genotyped. Sequences for genotyping primers are listed in
264 Supplemental Table 1. Generation of the *Neurog3*^{RG} BAC transgene and subsequent derivation
265 of the *Neurog3*^{RG2} mESC line and *Neurog3*^{RG2} reporter mice was described previously (6).
266 Although not previously reported in (6), mouse ES cells that stably integrated the *Neurog3*^{RG}
267 BAC LCA were analyzed by a qPCR-based assay that accurately estimates transgene copy
268 number (17). Briefly, we generated primers specific for the puromycin-resistance gene (Puro^R)
269 in the Puro^R- Δ TK-em7-Neo^R (Puro ^{Δ TK}) selection cassette in the *Neurog3*^{RG} transgene (Figure 2A).
270 Quantitative PCR was run on 2.5, 10, 20, 40 and 200 ng of genomic DNA from a TL1 mESC
271 knock-in line, carrying one copy of the Puro ^{Δ TK} cassette inserted via homologous recombination,
272 to yield a Δ C_T curve reflecting copy number (Figure 2B). Triplicate runs of exactly 20 ng of DNA
273 from 23 candidate *Neurog3*^{RG} mESC lines used the standard curve to define copy number.

274

275 **Generation of P2A.FUCCI transgene and the *Neurog3*^{P2A.FUCCI} reporter mouse line**

276 To generate the mKO2-hCdt1^(30/120)-P2A-mVenus-hGem^(1/110) (P2A.FUCCI) cassette, mKO2-
277 hCdt1^(30/120) and mVenus-hGem^(1/110) were PCR-amplified from plasmids provided by Dr. Atsushi
278 Miyawaki (RIKEN Brain Science Institute) (Sakaue-Sawano et al. 2008). Amplification of mKO2-
279 hCdt1^(30/120) involved attaching a 40 bp *Neurog3* homology region 5' of the mKO2 start codon
280 along with the first 25 base pairs of a P2A sequence 3' of mKO2. Amplification of mVenus-

281 hGem^(1/110) involved attaching a 5' BamHI site and a 3' Apal site. A third PCR was used to
282 generate a P2A cassette with 25 base pairs of the 3' end of mKO2-hCdt1^(30/120) attached to its 5'
283 end and a BamHI site at its 3' end. The resulting mKO2-hCdt1^(30/120) and P2A amplicons were
284 then fused together by overlap extension PCR (22), using a forward primer specific for the
285 mKO2-hCdt1^(30/120) amplicon and a reverse primer specific for the P2A amplicon. The resulting
286 mKO2-hCdt1^(30/120)-P2A amplicon was attached to the mVenus-hGem^(1/110) amplicon via the
287 BamHI site and inserted into a pBS KS(-) vector. The resulting P2A.FUCCI cassette was removed
288 from pBS KS (-) and inserted into a pCMV5 vector with a PGK-neomycin selection cassette for
289 expression in HeLa cells (described below). The P2A.FUCCI cassette was also inserted in place of
290 the RG cassette in the PL451-RG-FRT-Puro^R-ΔTK-em7-Neo^R-FRT-lox2272 vector described
291 previously (6). Using BAC recombineering the resulting P2A.FUCCI-FRT-Puro^R-ΔTK-em7-Neo^R-
292 FRT-lox2272 cassette was inserted immediately upstream of the Neurog3 start codon in the
293 Neurog3-containing RPCI-23-121F10 BAC (6). Using BAC recombineering, the P2A.FUCCI-FRT-
294 Puro^R-ΔTK-em7-Neo^R-FRT-lox2272 cassette was retrieved into a vector containing a lox66 site in
295 a manner that ensured that placement of the lox66 site precisely mimicked that of its lox71
296 counterpart in the lox71/lox2272 flanked *Neurog3*^{RG} BAC LCA. Subsequently, the FRT-flanked
297 Puro^R-ΔTK-em7-Neo^R cassette was replaced with an FRT-flanked PGK-Hygro^R selection cassette.
298 This final lox66/lox2272 flanked *Neurog3*^{P2A.FUCCI} exchange plasmid was linearized and used to
299 replace, via RMCE, the *Neurog3*^{RG} BAC LCA in the *Neurog3*^{RG2} mESC line. Successful replacement
300 with *Neurog3*^{P2A.FUCCI} was verified by PCR (Figure Supplement 2B). A single, verified,
301 *Neurog3*^{P2A.FUCCI} mES cell line was expanded, karyotyped and injected into blastocyst-stage
302 embryos to derive the *Neurog3*^{P2A.FUCCI} reporter mouse strain. The LCA capability of the

303 *Neurog3*^{RG1} mESC line was also tested and shown to allow efficient RMCE of lox66/lox2272
304 flanked cassettes (data not shown).

305

306 **Cell culture**

307 HeLa cells were cultured on tissue culture grade plastic at 37° C in Dulbecco's Modified Eagle
308 Medium (DMEM) supplemented with 10% fetal bovine serum (FBS), and 100 U/mL penicillin-
309 streptomycin. Cells were passaged by adding 0.05% trypsin-EDTA to a plate of semi-confluent
310 (<90%) cells. To test expression of the P2A.FUCCI reporter, HeLa cells were transiently
311 transfected with the *CMV*^{P2A.FUCCI} expression plasmid using Lipofectamine 2000 (Thermo Fisher)
312 according to manufacturer's instructions. The same conclusions were obtained with stable
313 clonal lines expressing *CMV*^{P2A.FUCCI} selected for neomycin resistance over 14 days (not shown).

314

315 **Immunodetection**

316 E14.5 dorsal pancreata were fixed in 4% paraformaldehyde (4 hrs, 4°C) then equilibrated in 30%
317 sucrose overnight at 4°C). A Leica CM3050S was used sucrose-equilibrated, OCT-embedded
318 tissue (Tissue-Tek) into 10 µm tissue sections, sequentially placed on three separate sets of
319 slides, each covering ~33% of the dorsal pancreas. Primary and Secondary antibodies are listed
320 in Supplemental Table 2. All images are epifluorescence from a Zeiss ApoTome microscope with
321 Zeiss Axiovision software.

322

323 **Flow sorting and qRT-PCR analysis**

324 Multiple E14.5 *Neurog3*^{P2A.FUCCI+} dorsal pancreata were pooled and dispersed into a single-cell
325 suspension using Accumax (Sigma) (protocol available on request). Dispersed samples were
326 washed and incubated on ice, first with Muc1 antibody for 1 hr, then anti-hamster Cy5
327 secondary antibody for an additional hour. DAPI was added to ensure sorting of viable cells.
328 Flow sorting used a BD FACSAria III. cDNA was generated using iScript cDNA synthesis kit (Bio-
329 Rad) from RNA isolated from flow-sorted cells after TRIzol extraction. PCR was performed in a
330 Bio-Rad CFX96 with SsoFast EvaGreen Supermix (Bio-Rad) using at least three technical
331 replicates. Relative expression level (normalized to *Gapdh*) was calculated by first assessing the
332 ΔC_T between the gene of interest and *Gapdh* before converting the ΔC_T to relative expression
333 level ($2^{\Delta C_T}$). The results in Figure 4 were independently repeated (biological replicate) with
334 similar results. Primer sequences, except for *Insm1* primers (Applied Biosystems), are listed in
335 Supplemental Table 1.

336

337 **Quantification and statistics**

338 Cell counting and fluorescence intensity quantifications were done using NIH ImageJ software.
339 For quantifications “n” indicates total cells counted, with “N” number of individual dorsal
340 pancreata analyzed. As previously stated approximately 33% of an entire dorsal pancreas was
341 analyzed for each dorsal pancreas. Previous reports indicate that only 2% of the total pancreas
342 volume needs to be systematically sampled and analyzed to obtain a relative error of $\leq 10\%$
343 (**23**). Error bars generated using standard error of the mean (SEM), with Student’s t-test (one-
344 tailed) used to calculate *p* values. *p* values were deemed significant when ≤ 0.05 .

345

346 **Acknowledgements**

347 We thank Atsushi Miyawaki (RIKEN Brain Science Institute) for the mKO2-hCdt1^(30/120)/pCSII-EF-
348 MCS and mVenus-hGem^(1/110)/pCSII-EF-MCS plasmids. This work utilized the Cell Imaging Shared
349 Resource and Transgenic/ES Cell Shared Resource core facilities of the Vanderbilt Diabetes
350 Research and Training Center funded by NIDDK grant 020593. Flow cytometry was performed
351 in the VUMC Flow Cytometry Shared Resource supported by the Vanderbilt-Ingram Cancer
352 Center (P30 CA68485) and the Vanderbilt Digestive Disease Research Center (DK0558404).
353 Generation of *Neurog3*^{RG2} and *Neurog3*^{P2A.FUCCI} mice was supported in part by the Beta Cell
354 Biology Consortium Mouse ES Cell Core funded by the NIDDK (U01DK072473). We thank Anna
355 Means, Guoqiang Gu, and members of the Wright/Gu labs for discussions. This study was
356 supported by the NIH/NIDDK (U01DK089570) and an American Heart Association fellowship to
357 MB (13POST14240011).

358

359 **Competing Interests**

360 The authors declare that no competing interests exist.

361

362

363 References

- 364 1. **Gradwohl G, Dierich A, LeMeur M, Guillemot F.** 2000. Neurogenin3 Is Required for the
365 Development of the Four Endocrine Cell Lineages of the Pancreas. *Proc Natl Acad Sci U S*
366 *A* **97**:1607–1611.
- 367 2. **McGrath PS, Watson CL, Ingram C, Helmrath MA, Wells JM.** 2015. The Basic Helix-Loop-
368 Helix Transcription Factor NEUROG3 Is Required for Development of the Human
369 Endocrine Pancreas. *Diabetes* **64**:2497–505.
- 370 3. **Miyatsuka T, Kosaka Y, Kim H, German MS.** 2011. Neurogenin3 inhibits proliferation in
371 endocrine progenitors by inducing Cdkn1a. *Proc Natl Acad Sci* **108**:185–190.
- 372 4. **Wang S, Yan J, Anderson DA, Xu Y, Kanal MC, Cao Z, Wright CVE, Gu G.** 2010. Neurog3
373 gene dosage regulates allocation of endocrine and exocrine cell fates in the developing
374 mouse pancreas. *Dev Biol* **339**:26–37.
- 375 5. **Johansson KA, Dursun U, Jordan N, Gu G, Beermann F, Gradwohl G, Grapin-Botton A.**
376 2007. Temporal Control of Neurogenin3 Activity in Pancreas Progenitors Reveals
377 Competence Windows for the Generation of Different Endocrine Cell Types. *Dev Cell*
378 **12**:457–465.
- 379 6. **Bechard ME, Bankaitis ED, Hipkens SB, Ustione A, Piston DW, Yang Y-P, Magnuson MA,**
380 **Wright CVE.** 2016. Precommitment low-level Neurog3 expression defines a long-lived
381 mitotic endocrine-biased progenitor pool that drives production of endocrine-committed
382 cells. *Genes Dev* **30**:1852–1865.
- 383 7. **Bankaitis ED, Bechard ME, Wright CVE.** 2015. Feedback control of growth,
384 differentiation, and morphogenesis of pancreatic endocrine progenitors in an epithelial
385 plexus niche. *Genes Dev* **29**:2203–2216.
- 386 8. **Roybon L, Hjalt T, Stott S, Guillemot F, Li J-Y, Brundin P.** 2009. Neurogenin2 directs
387 granule neuroblast production and amplification while NeuroD1 specifies neuronal fate
388 during hippocampal neurogenesis. *PLoS One* **4**:e4779.
- 389 9. **Shimojo H, Ohtsuka T, Kageyama R.** 2011. Dynamic Expression of Notch Signaling Genes
390 in Neural Stem/Progenitor Cells. *Front Neurosci* **5**:1–7.
- 391 10. **Ali F, Hindley C, McDowell G, Deibler R, Jones A, Kirschner M, Guillemot F, Philpott A.**
392 2011. Cell cycle-regulated multi-site phosphorylation of Neurogenin 2 coordinates cell
393 cycling with differentiation during neurogenesis. *Development* **138**:4267–4277.
- 394 11. **Florio M, Leto K, Muzio L, Tinterri A, Badaloni A, Croci L, Zordan P, Barili V, Albieri I,**
395 **Guillemot F, Rossi F, Consalez GG.** 2012. Neurogenin 2 regulates progenitor cell-cycle
396 progression and Purkinje cell dendritogenesis in cerebellar development. *Development*
397 **139**:2308–2320.
- 398 12. **Hindley C, Ali F, McDowell G, Cheng K, Jones A, Guillemot F, Philpott A.** 2012. Post-

- 399 translational modification of Ngn2 differentially affects transcription of distinct targets to
400 regulate the balance between progenitor maintenance and differentiation. *Development*
401 **139**:1718–1723.
- 402 13. **Bechard ME, Wright CVE.** 2017. New ideas connecting the cell cycle and pancreatic
403 endocrine-lineage specification. *Cell Cycle* **16**:301–303.
- 404 14. **Krentz NAJ, van Hoof D, Li Z, Watanabe A, Tang M, Nian C, German MS, Lynn FC.** 2017.
405 Phosphorylation of NEUROG3 Links Endocrine Differentiation to the Cell Cycle in
406 Pancreatic Progenitors. *Dev Cell* **41**:129–142.
- 407 15. **Azzarelli R, Hurley C, Sznurkowska MK, Rulands S, Hardwick L, Gamper I, Ali F,**
408 **McCracken L, Hindley C, McDuff F, Nestorowa S, Kemp R, Jones K, Göttgens B, Huch M,**
409 **Evan G, Simons BD, Winton D, Philpott A.** 2017. Multi-site Neurogenin3 Phosphorylation
410 Controls Pancreatic Endocrine Differentiation. *Dev Cell* **274**–286.
- 411 16. **Sakaue-Sawano A, Kurokawa H, Morimura T, Hanyu A, Hama H, Osawa H, Kashiwagi S,**
412 **Fukami K, Miyata T, Miyoshi H, Imamura T, Ogawa M, Masai H, Miyawaki A.** 2008.
413 Visualizing Spatiotemporal Dynamics of Multicellular Cell-Cycle Progression. *Cell*
414 **132**:487–498.
- 415 17. **Chandler KJ, Chandler RL, Broeckelmann EM, Hou Y, Southard-Smith EM, Mortlock DP.**
416 2007. Relevance of BAC transgene copy number in mice: Transgene copy number
417 variation across multiple transgenic lines and correlations with transgene integrity and
418 expression. *Mamm Genome* **18**:693–708.
- 419 18. **Abe T, Sakaue-Sawano A, Kiyonari H, Shioi G, Inoue K, Horiuchi T, Nakao K, Miyawaki A,**
420 **Aizawa S, Fujimori T.** 2013. Visualization of cell cycle in mouse embryos with Fucci2
421 reporter directed by Rosa26 promoter. *Development* **140**:237–246.
- 422 19. **Mellitzer G, Martín M, Sidhoum-Jenny M, Orvain C, Barths J, Seymour P a, Sander M,**
423 **Gradwohl G.** 2004. Pancreatic islet progenitor cells in Neurogenin 3-yellow fluorescent
424 protein knock-add-on mice. *Mol Endocrinol* **18**:2765–76.
- 425 20. **Huang HP, Liu M, El-Hodiri HM, Chu K, Jamrich M, Tsai MJ.** 2000. Regulation of the
426 pancreatic islet-specific gene BETA2 (NeuroD) by Neurogenin 3. *Mol Cell Biol* **20**:3292–
427 3307.
- 428 21. **Gasa R, Mrejen C, Lynn FC, Skewes-Cox P, Sanchez L, Yang KY, Lin CH, Gomis R, German**
429 **MS.** 2008. Induction of pancreatic islet cell differentiation by the Neurogenin-NeuroD
430 cascade. *Differentiation* **76**:381–391.
- 431 22. **Horton RM, Cai Z, Ho SN, Pease LR.** 2013. Gene splicing by overlap extension: Tailor-
432 made genes using the polymerase chain reaction. *Biotechniques* **54**:528–535.
- 433 23. **Chintinne M, Stangé G, Denys B, In 'T Veld P, Hellemans K, Pipeleers-Marichal M, Ling**
434 **Z, Pipeleers D.** 2010. Contribution of postnatally formed small beta cell aggregates to
435 functional beta cell mass in adult rat pancreas. *Diabetologia* **53**:2380–2388.